

Time representation in neural network models trained to perform interval timing tasks

Zedong Bi^a and Changsong Zhou^{a,b,c,d,1}

^aDepartment of Physics, Centre for Nonlinear Studies and Institute of Computational and Theoretical Studies, Hong Kong Baptist University, Kowloon Tong, Hong Kong, China

^bResearch Centre, HKBU Institute of Research and Continuing Education, Shenzhen, China

^cBeijing Computational Science Research Center, Beijing, China

^dDepartment of Physics, Zhejiang University, 38 Zheda Road, Hangzhou, China

¹E-mail: cszhou@hkbu.edu.hk

October 14, 2021

Abstract

To predict and maximize future rewards in this ever-changing world, animals must be able to discover the temporal structure of stimuli and then take the right action at the right time. However, we still lack a systematic understanding of the neural mechanism of how animals perceive, maintain, and use time intervals ranging from hundreds of milliseconds to multi-seconds in working memory and appropriately combine time information with spatial information processing and decision making. Here, we addressed this problem by training neural network models on four timing tasks: interval production, interval comparison, timed spatial reproduction, and timed decision making. We studied time-coding principles of the network after training, and found them consistent with existing experimental observations. We reveal that neural networks perceive time intervals through the evolution of population state along a stereotypical trajectory, maintain time intervals by line attractors along which the activities of most neurons vary monotonically with the duration of the maintained interval, and adjust the evolution speed of the state trajectory for producing or comparing time intervals. Spatial information or decision choice preserves the profiles of neuronal activities as functions of time intervals maintained in working memory or flow of time, and is coded in the amplitudes of these profiles. Decision making is combined with time perception through two firing sequences with mutual inhibition. Our work discloses fundamental principles of the neuronal coding of time that supports the brain for flexible temporal processing. These principles facilitate generalizable decoding of time and non-time information.

Keywords— interval timing, population coding, neural network model

Significance

Flexible timing requires the ability to perceive, maintain, and use time intervals ranging from hundreds of milliseconds to multi-seconds in working memory combined with spatial information and decision making to act or anticipate appropriately at the right time. To understand the neural mechanisms of timing, we trained neural networks to perform basic and combined timing tasks. After training, the neural networks perceived time intervals through states along stereotypical trajectories, maintained time intervals by attractor dynamics, and temporally scaled neuronal activity profiles according to the maintained time interval for further timing tasks. Spatial information or decision choice was coded orthogonally in the amplitudes of neuronal firing profiles with time information. These findings reveal fundamental strategies of neuronal coding of time.

Introduction

Much information that the brain processes and stores is temporal in nature. Therefore, to understand the processing of time in the brain is of fundamental importance in neuroscience [1, 2, 3, 4]. Working memory, the ability to maintain and manipulate information over a period of seconds, is a core cognitive function for planning and executing tasks [5, 6]. In this study, we focused on the working memory of a basic temporal pattern: time interval.

To predict and maximize future rewards in this ever-changing world, animals must be able to discover the temporal structure of stimuli and then take the right action at the right time. To this end, animals must be able to perceive, maintain, and then use time intervals in working memory, appropriately combining the processing of time with spatial information and decision making. Based on behavioral data and the diversity of neuronal response profiles, it has been proposed [7, 8] that time intervals in the range of hundreds of milliseconds to multi-seconds can be decoded through neuronal population states evolving along transient trajectories. The neural mechanisms may be accumulating firing [9, 10], synfire chains [11, 12], or the beating of a range of oscillation frequencies [13]. However, these mechanisms are challenged by recent finding that animals can flexibly adjust

the evolution speed of population activity along an invariant trajectory to produce different intervals [14]. Through behavioral experiments, it was found that humans can store time intervals as distinct items in working memory in a resource allocation strategy [15], but an electrophysiological study on the neuronal coding of time intervals maintained in working memory is still lacking. Moreover, increasing evidence indicates that timing does not rely on dedicated circuits in the brain, but instead is an intrinsic computation that emerges from the inherent dynamics of neural circuits [16, 3]. Spatial working memory and decision making are believed to rely mostly on a prefrontalparietal circuit [17, 18]. How this circuit combines spatial working memory and decision making with temporal processing remains unclear. Overall, our understanding of the processing of time intervals in the brain is fragmentary and incomplete. It is therefore essential to develop a systematic understanding of the fundamental principle of temporal processing and its combination with spatial information and decision making. In this study, therefore, we trained artificial neural networks (ANN) on several basic and combined timing tasks.

Previous works showed that after being trained to perform tasks such as categorization, working memory, decision making, and motion generation, ANN exhibited coding or dynamic properties surprisingly similar to experimental observations [19, 20, 21, 22]. Compared to animal experiments, ANN can cheaply and easily implement a series of tasks, greatly facilitating the capture of common computational principles underlying these tasks [23, 24]. Unlike previous works, which only discussed interval production using ANN [14, 25], we studied the perception, maintenance, and production of time intervals, as well as their combination with spatial information and decision-making processes, using a series of tasks. We found that neural networks perceive, maintain, and produce time intervals using different computational strategies and that spatial information or decision choice preserves the shapes of neuronal firing profiles with time information. These strategies facilitate generalizable decoding of time and non-time information.

Results

Model setup

In our simulation, we used vanilla recurrent neural networks of units with the softplus activation function, which is very similar to neuronal current-rate curves after re-parameterization [26]. We trained the networks on four interval timing tasks (**Fig. 1**): interval production (IP), timed spatial reproduction (t-SR), timed decision making (t-DM), and interval comparison (IC). In IP, two pulses are successively presented with interval T in between; then, a Go cue appears after a random delay period, and an action is to be produced at time T after the Go cue. In t-SR, the first pulse contains information of a spatial direction, and at time T after the Go cue, an action is to be produced toward the spatial direction indicated by the first pulse. In t-DM, two noisy inputs are simultaneously presented lasting for T time, and the network should indicate which input is stronger at time T after a Go-cue pulse. In IC, two lasting stimuli are successively presented, and the network should indicate which stimulus has a longer duration. The first three tasks have three epochs (the first three tasks in **Fig. 1**): perception, delay, and production epochs. The IC task has four epochs (the last task in **Fig. 1**): stimulus1, delay, stimulus2, and go epochs. Through IP and IC, we studied how timing intervals are perceived, maintained, and then used by the network. Through t-SR and t-DM, we studied how time information is combined with spatial information and the decision-making process so that the network can perform the appropriate action at the right time.

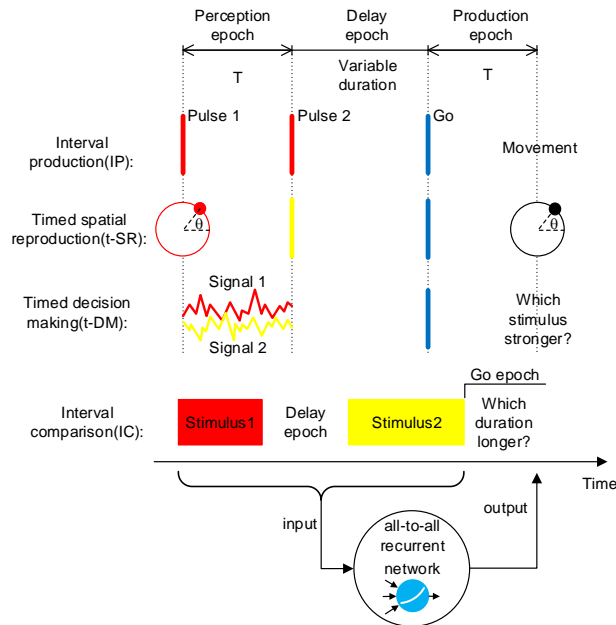


Figure 1: **Model setup.** All-to-all connected recurrent networks with softplus units are trained on four timing tasks. Stimuli with different colors (red, yellow, or blue) indicate that they are input to the network through different synaptic weights. See **Figs S1a–d** for performance examples after training.

Interval production task

In an interval production task (first task of **Fig. 11**), the network should perceive the interval between the first two pulses, maintain the interval during the delay epoch, and then produce it after the Go cue. In this section, we report on the dynamics of the network that supports perception, maintenance, and production of time interval.

The first epoch is the perception epoch. In the subspace spanned by the first three principal components (PCs) in different simulation trials, the network started to evolve from almost the same state along an almost identical trajectory in response to the first stimulus pulse until another pulse came (**Fig. 2a**); the activities of individual neurons before the second pulse in different trials highly overlapped (**Figs. 2b, c**). Therefore, the network perceived the interval from the beginning of the perception epoch using states along a stereotypical trajectory. Behaviorally, a humans perception of the time interval between two acoustic pulses is impaired if a distractor pulse appears shortly before the first pulse [27]. A modeling work [27] explained that this is because successful perception requires the network state to start to evolve from near state a in response to the first pulse, whereas the distractor pulse kicks the network state far away from a . This explanation is consistent with our results that interval perception requires a stereotypical trajectory.

We then studied how the information of timing interval T between the first two pulses was maintained during the delay epoch. We noted two properties of the trajectories in the delay epoch from the subspace spanned by the first three PCs (**Fig. 2d**): (1) the speeds of the trajectories decreased with time (**Fig. 2e**) and (2) the states at the end of the delay epoch at different T s were aligned in a low-dimensional manifold \mathcal{M} because the first PC of \mathcal{M} explained 90% of its variance (**Fig. 2f**). Therefore, \mathcal{M} approximated a line attractor [28, 21]: trajectories were attracted toward \mathcal{M} near which dynamics were slow, and T was encoded as the position on \mathcal{M} . To better understand the scheme of coding T around \mathcal{M} , we classified neuronal activity $f(T)$ as a function of T at the end of the delay epoch into three types (**Fig. 2g**): monotonically decreasing (MoD), monotonically increasing (MoI), and middle peaking (MiP) (see Methods for details). We found that most neurons were MoD or MoI, whereas only a small portion were MiP neurons (**Fig. 2h**). This implies that the network mainly used a complementary (i.e., concurrently increasing and decreasing) monotonic scheme to code time intervals in the delay epoch, similar to the scheme revealed in experiments to code another one-dimensional sensory stimuli: somatosensory vibration frequency [29]. This dominance of monotonic neurons may be the reason why the first PC of \mathcal{M} explained so much variance (**Fig. 2f**), see SI Text and **Figs. S2e, f** for a simple explanation.

In the production epoch, in the subspace of the first three PCs, the trajectories of the different T values tended to be isomorphic (**Fig. 2i**). The neuronal activity profiles were self-similar when stretched or compressed in accordance with the produced interval (**Fig. 2j**), suggesting temporal scaling with T [14]. To quantify this temporal scaling, we defined the scaling index (SI) of a subspace \mathcal{S} as the portion of variance of the projections of trajectories into \mathcal{S} that can be explained by temporal scaling [14]. We then used a dimensionality reduction technique that furnished a set of orthogonal directions (called scaling components, or SCs) that were ordered according to their SI (see Methods). We found that a subspace (spanned by the first three SCs) that had high SI ($=0.98$) occupied about 40% of the total variance of trajectories (**Fig. 2k**). The average velocity of the trajectory in the subspace of the first three SCs was inversely proportional to T (**Fig. 2l**). This implies that the network adjusted its dynamic velocity to produce different time intervals in the production epoch, similar to observations of the medial frontal cortex of monkeys [25, 14].

We then investigated the functional overlap of the three epochs, assessing whether a neuron could be engaged in only one epoch, in every epoch, or between these two extreme scenarios. To this end, we studied the overlap between sets of strongly active neurons (i.e., neurons whose peak firing rates were larger than a threshold) in different epochs. We found a partially mixed scenario (**Fig. 2m**): although some neurons were strongly active in only one epoch, most neurons were strongly active in two or all three epochs.

In all three epochs of the interval production task, we found that a common feature of network dynamics was neuronal sequential firing (**Fig. 2n, Figs. S2a, c**). We measured the recurrent weight $W(i-j)$ as a function of the difference $i-j$ of orders of peak firing time between two neurons and found, on average, stronger connections from earlier- to later-peaking neurons than from later- to earlier-peaking neurons in all three epochs (**Fig. 2o, Figs. S2b, d**) [30, 31, 11]. We also studied the overlap of network dynamics of the three epochs, assessing whether the fact that neuron a peaks before neuron b in one epoch implies that a also peaks before b in another epoch. To this end, we picked neurons that were strongly active in both of two different epochs and tested the significance that the similarity of firing sequences of these neurons in the two epochs was larger than chance [32]. Interestingly, for any two of the three epochs, the p value was far larger than 0.05 in most cases (**Fig. 2p**). This means that there was nearly no similarity between the firing sequences of the two different epochs. In other words, although the sets of neurons involved in different epochs largely overlapped (**Fig. 2m**), the dynamic interaction of these neurons could be flexibly reconfigured to support a variety of functional roles.

Interval comparison task

In the interval comparison task (last task in **Fig. 1**), the network was successively presented with two intervals; it was then required to judge which interval was longer. In the stimulus1 epoch, population activity evolved along a stereotypical trajectory from the beginning of the first stimulus until the first stimulus ended after time T (**Fig. 3a**). In the delay epoch, trajectories were attracted toward a low-dimensional manifold, with velocity decreasing with time (**Figs. 3b, c**). At the end of the delay epoch, the activities of most neurons changed monotonically with T (**Fig. 3d**). The population trajectory in the stimulus2 epoch had a critical time point: time T after the start of the stimulus2 epoch. The network should give different comparison outputs at the Go epoch depending on whether the trajectory in the stimulus2 epoch had passed over this critical point. Interestingly, we found that critical points in the trajectories with different T values were spatially close (**Fig. 3e**). The trajectories from the start of the stimulus2 epoch to the critical points had a subspace with high temporal scaling (SI=0.98) that could explain 50% of the total variance (**Fig. 3f**). The average velocity of the trajectories in the subspace of the first three scaling components was inversely proportional to T (**Fig. 3g**).

The interval production (IP) and interval comparison (IC) tasks have two differences. The first is the task requirement. The second is that in IP, the time interval is defined by two pulses, whereas in IC, the time interval is defined by a lasting stimulus.

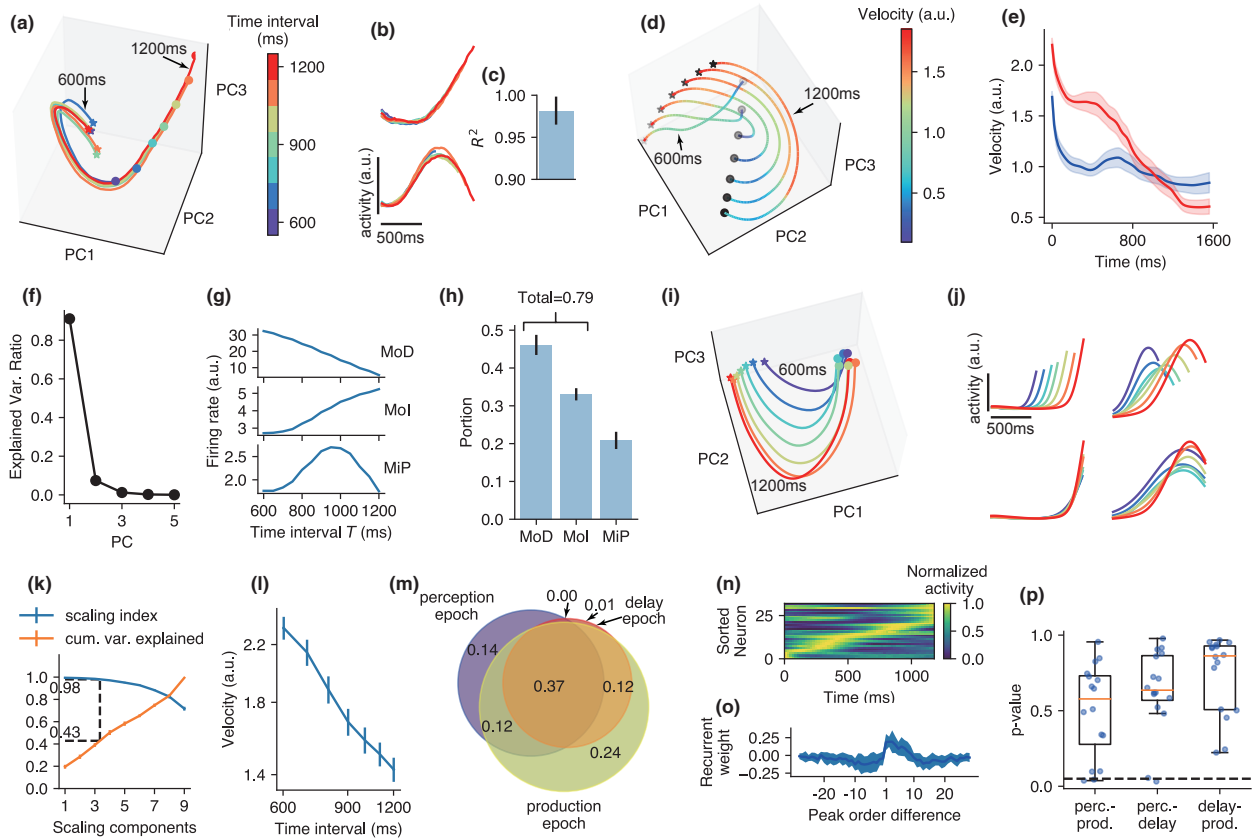


Figure 2: Interval production task. (a) Population activity in the perception epoch in the subspace of the first three PCs. Colors indicate the time interval T between the first two pulses. Stars and circles respectively indicate the starting and ending points of the perception epoch. The trajectories for $T = 600$ ms and 1200 ms are labeled. (b) Firing profiles of two example neurons in the perception epoch. The colors of the lines have the same meaning as in panel a. (c) Coefficient of determination (R^2) of how much the firing profile with the largest T can explain the variance of firing profiles with smaller T in the perception epoch. The error bar indicates s.d. over different neurons and T values. (d) Population activity in the subspace of the first three PCs in the delay epoch. Colors indicate the trajectory velocity. The increasing blackness of stars and circles indicates trajectories with $T = 600$ ms, 700 ms, ..., 1200 ms. (e) Trajectory velocity as a function of time in the delay epoch when $T = 600$ ms (blue) and 1200 ms (red). Shaded belts indicate s.e.m. (standard error of mean) over training configurations. (f) Ratio of explained variance of the first five PCs of the set \mathcal{M} of ending points of the delay epoch with different T values. Error bars that indicate s.e.m. are smaller than plot markers. (g) Firing rates of three example neurons of monotonically decreasing (MoD), monotonically increasing (MoI), and middle peaking (MiP) types as functions of T at the end of the delay epoch. (h) The portions of the three types of neurons. (i) Population activity in the production epoch in the subspace of the first three PCs. Colors indicate the time intervals to be produced, as shown in the color bar of panel a. Stars and circles respectively indicate the starting and ending points of the production epoch. (j) Upper: firing profiles of two example neurons in the production epoch. Lower: firing profiles after temporal scaling according to produced intervals. (k) A point at horizontal coordinate x means the scaling index (blue) or ratio of explained variance (orange) of the subspace spanned by the first x scaling components (SCs). Dashed lines indicate that a subspace with scaling index 0.98 explains, on average, 43% of the total variance. (l) Trajectory velocity in the subspace of the first three SCs as the function of the time interval to be produced. (m) Venn diagram showing the overlap (portion indicated by number) between sets of strongly active neurons in different epochs. (n) An example of neuronal activity (with maximum normalized to 1) in the perception epoch sorted according to peak time. (o) The mean (solid line) and s.d. (shaded belt) of the recurrent weights as a function of the peak order difference between post- and pre-synaptic neurons in the perception epoch. (p) The significance of the hypothesis that the sequential firing orders are more similar than chance in any two of the three epochs: perception (perc.), delay, and production (prod.) epochs. Dashed line means the significance threshold $p = 0.05$. Whisker plots: center line, median; box, 25th to 75th percentiles; whiskers $\pm 1.5 \times$ the interquartile range; dots, p values of all 16 training configurations. In panels h, k, and l, error bars indicate s.e.m. over training configurations. During training, we added recurrent and input noises. When analyzing the network properties after training, we turned off noises for the delay and production epochs but kept noises for the perception epoch. Without noise, the trajectories in the perception epoch would fully overlap under different simulation conditions.

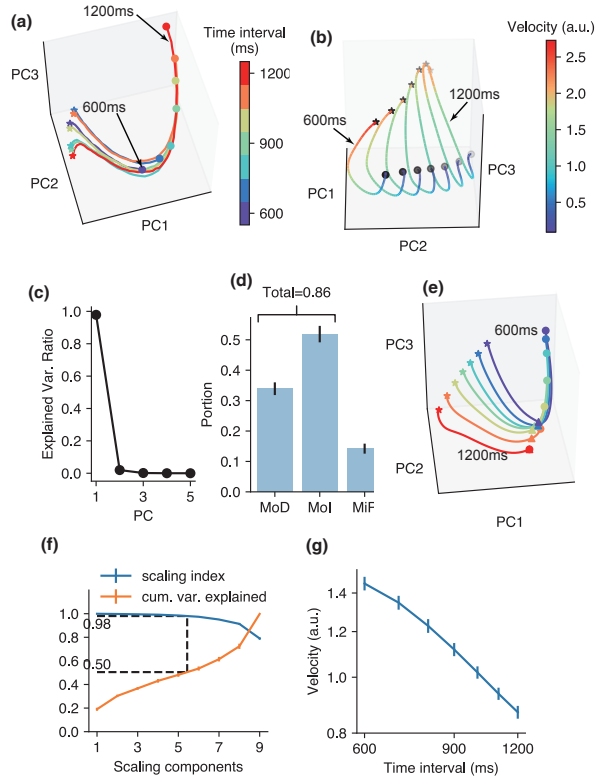


Figure 3: **Interval comparison task.** (a) Population activity in the stimulus1 epoch in the subspace of the first three PCs. Colors indicate the time duration T of the first stimulus. Stars and circles respectively indicate the starting and ending points of the stimulus1 epoch. (b) Population activity in the delay epoch in the subspace of the first three PCs. Colors indicate velocity. The increasing blackness of stars and circles indicates $T = 600$ ms, 700 ms, \dots , 1200 ms. (c) Ratio of explained variance of the first five PCs of the set of ending points \mathcal{M} of the delay epoch at different T values. (d) Portions of the three types of neurons at the end of the delay epoch. (e) Population activity in the stimulus2 epoch in the subspace of the first three PCs. Colors represent the time duration T of the first stimulus (see color bar in panel a). The second stimulus has a duration of 1200 ms. Stars and circles respectively indicate the starting and ending points of the stimulus2 epoch. Triangles indicate critical points. (f) Investigation of temporal scaling of the trajectories from the start of the stimulus2 epoch to the critical points. (g) Trajectory velocity in the subspace of the first three SCs as a function of duration T of stimulus1. In panels d, f, g, error bars mean s.e.m. over training configurations.

Despite these differences, we can see strong similarities in the schemes the network developed to perceive, maintain, and use time interval information: to perceive it with a stereotypical trajectory, to maintain using attractor dynamics with a complementary monotonic coding scheme, and to use it with velocity adjustment. These similarities imply universal computational schemes in neural networks for temporal information processing.

Timed spatial reproduction task

In the timed spatial reproduction task (second task in Fig. 1), the network should not only take action at the desired time but also act toward the direction indicated by the first pulse. The network should deal with two types of time information: temporal flow and time interval. In the perception or production epoch, the network should constantly estimate the interval between the starting point of the epoch and the present time: this is the information of temporal flow. In the delay or production epoch, the network should maintain the information of the duration of the perception epoch: this is the information of time interval. From our previous discussion, temporal flow is coded using state evolution with time; the time interval is coded using an attractor in the delay epoch and a trajectory velocity in the production epoch. In the following, we will discuss the coding combination of spatial information with temporal flow and time interval.

In the perception epoch, in response to the first pulse at a given direction θ , the network evolved along a stereotypical trajectory until the second pulse came after time T (Figs 4a, b). The profiles of the trajectories with different θ s in the subspace of the first three PCs looked spatially organized (Fig. 4b), suggesting that neuronal activities at different θ s should not be independent. Consistently, the activity of a neuron at different θ s also shared similar temporal profiles (Fig. 4c), especially when two θ s had close values. Notably, in our simulation, the direction of the first pulse was represented by a Gaussian bump centered at θ with standard deviation $\pi/8$, which is much smaller than the smallest angular difference $\pi/3$ between different colors in Figs 4a, b, c; thus, the similarity of the temporal profiles in Figs. 4b, c should not result from overlap of angular inputs of the first pulse but rather emerge during training. To quantitatively confirm this similarity, we compared the temporal profiles of neuronal activities in two of the most dissimilar cases: opposite directions. Specifically, we studied the peak time $t_i^{peak}(\theta)$ of neuron i at direction θ and peak time $t_i^{peak}(\theta + \pi)$ at the opposite direction $\theta + \pi$. We found

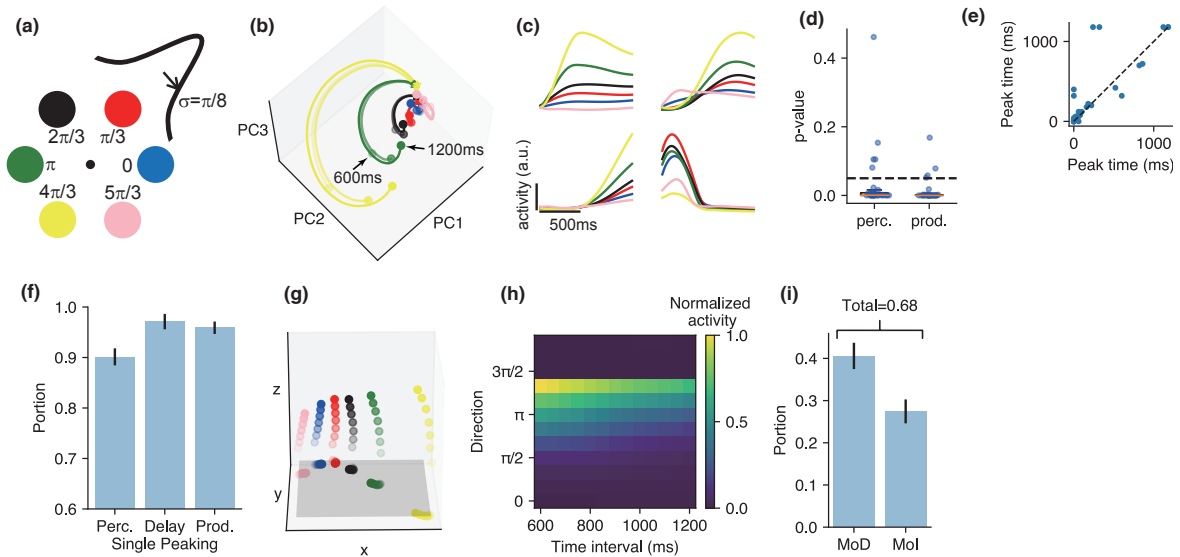


Figure 4: Timed spatial reproduction task. (a) Color scheme that represents the direction of the first pulse, used in panels b, c, g. In our simulation, direction was represented by a Gaussian bump with standard deviation $\pi/8$. (b) Trajectory of the perception epoch in the subspace of the first three PCs. Lines with decreasing opacity represent trajectories when $T = 600$ ms, 900 ms, and 1200 ms. (c) Firing profiles of four example neurons in the perception epoch. (d) P value of the significance that $|t_i^{peak}(\theta) - t_i^{peak}(\theta + \pi)|$ is smaller than chance. In the perception (perc.) and production (prod.) epochs, $\theta = 0$, or $\pi/2$. Whisker plots: red center line, median; box, 25th to 75th percentiles; whiskers, $\pm 1.5 \times$ the inter-quartile range; dot, p value for the setting of parameters in a training configuration. Boxes and whiskers may be too short to recognize. Dashed horizontal line indicates $p = 0.05$. $T = 1200$ ms. (e) $t_i^{peak}(\theta)$ vs $t_i^{peak}(\theta + \pi)$ across i in an example training configuration. Note that some dots are located near the diagonal dashed line. Interval of perception epoch $T = 1200$ ms. (f) Portion of neurons whose maximal activity with θ in the perception epoch, the production epoch, or at the end of the delay epoch is single-peaking. (g) Population states at the end of the delay epoch in the subspace of the first three PCs. Colors indicate directions shown in panel a. Increasing opacities indicate time intervals between the first two pulses $T = 600$ ms, 700 ms, \dots , 1200 ms. The z -axis is chosen to be the direction most aligned to the change of population state with T , and x and y are two axes orthogonal to z . Projections into the x - y plane are also plotted. (h) Activity of an example neuron at the end of the delay epoch as a function of θ and T . (i) Portion of neurons whose activity at the end of the delay epoch are monotonically decreasing (MoD) and monotonically increasing (MoI) with T . In panels f, i, the error bar indicates s.e.m. over training configurations.

that for most training configurations, $|t_i^{peak}(\theta) - t_i^{peak}(\theta + \pi)|$ had a significantly smaller value than chance (**Fig. 4e, first column of d**). This implies that in the perception epoch, neuronal temporal profiles largely preserved their shapes at different θ s, and the information of θ was largely coded in the amplitudes of temporal profiles. To understand the coding of θ , we defined $h_i(\theta)$ as the highest activity of neuron i in the perception epoch at θ , and classified $h_i(\theta)$ into two types: single peaking and multi-peaking, depending on the number of peaks of $h_i(\theta)$. We found that most neurons had single-peaking tuning with θ (**Fig. 4, first column of f**). We also studied the coding of temporal flow and θ in the production epoch, and got similar results (**Fig. 4, second column of d, last column of f**).

In the delay epoch, trajectories were attracted toward a manifold of slow dynamics (**Fig. S3a**). In the subspace of the first three PCs, at different θ values, the state at the end of the delay epoch tended to change with T along the same direction (z -axis in **Fig. 4g**), and θ was coded by a circular position in the subspace largely vertical to this direction (x - y plane in **Fig. 4g**). We then studied the tuning $f_i(\theta, T)$ of the i th neuron with θ and T at the end of the delay epoch. As for the tuning property with T , we called neuron i monotonically decreasing (MoD) or monotonically increasing (MoI) with T only if $f_i(\theta, T)$ is a MoD or MoI function, respectively, with T at any θ value where neuron i can reach high activity. As for the tuning property with θ , we defined $g_i(\theta) = \max_T f_i(\theta, T)$ as the highest activity of neuron i at θ at the end of the delay epoch and calculated the number of peaks of $g_i(\theta)$. We found that most neurons had monotonic tuning with T (**Fig. 4i**) and single-peaking tuning with θ (**Fig. 4, middle column of f**). See **Fig. 4h** for $f_i(\theta, T)$ of an example neuron.

In the production epoch, when the duration of the perception epoch was different, neuronal temporal profiles were accordingly scaled and the trajectory velocity was accordingly adjusted (**Figs. S3b, c**). Therefore, similar to the interval production task, the time interval was coded using trajectory velocity in the production epoch.

Collectively, maintaining the information of θ in the first pulse did not change the temporal profiles in the perception and production epochs used to code temporal flow, and it did not change the complementary monotonic coding scheme in the delay epoch and the scaling property in the production epoch used to code time intervals. The information of θ was coded in the amplitudes of temporal profiles in the perception and production epochs, as well as the amplitudes of monotonic tuning with T in the delay epoch, in a single-peaking manner.

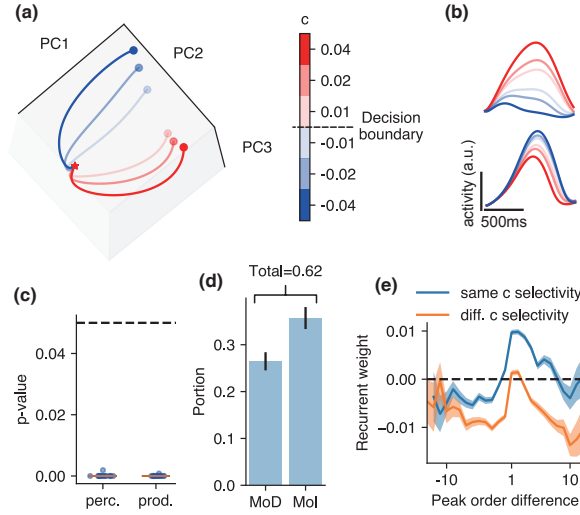


Figure 5: **Timed decision-making task.** (a) Trajectories in the perception epoch in the subspace of the first three PCs. Colors indicate c value. (b) Firing profiles of two example neurons in the perception epoch, which respectively increases with c (upper) and decreases with c (lower). (c) P value of the significance that $|t_i^{peak}(c = 0.01) - t_i^{peak}(c = -0.01)|$ is smaller than chance in the perception (perc.) and production (prod.) epochs. Whisker plots: red center line, median; box, 25th to 75th percentiles; whiskers, $\pm 1.5 \times$ the inter-quartile range; dot, p value for a setting of parameters in a training configuration. Dashed horizontal line indicates $p = 0.05$. Boxes and whiskers may be too short to recognize. Interval of perception epoch $T = 1200$ ms. (d) The portion of neurons whose activity at the end of the delay epoch is monotonically decreasing (MoD) and monotonically increasing (MoI) with T , at both $c < 0$ and $c > 0$. (e) Recurrent weight connection from a reference neuron to the other strongly active neurons of the same (blue) or different (orange) types as a function of the difference between peak order from the reference neuron. The shaded belt indicates s.e.m. In panel d, the error bar indicates s.e.m. over training configurations. During training, we added recurrent and input noises, but we turned off noises for data analysis after training.

Timed decision-making task

In the timed decision-making task (third task in Fig. 1), the network should make a decision choice at the desired time. We denoted c as the half-difference between the strengths of the two stimuli, and the network should make different decisions depending on whether c is positive or negative.

Similar to the timed spatial reproduction task, we found that decision choice preserved the neuronal firing profiles with both temporal flow and time interval. Neuronal temporal profiles at different c values in the perception and production epochs looked similar (Figs. 5a, b), which was quantitatively confirmed by the fact that the difference $|t_i^{peak}(c > 0) - t_i^{peak}(c < 0)|$ between peak times t_i^{peak} of the temporal profiles when $c > 0$ and $c < 0$ was significantly smaller than chance ($p < 0.05$) (see Fig. 5c). For most neurons, the tuning $f(T, c)$ at the end of the delay epoch with T and c was monotonic with T , and this monotonicity did not change with c (Fig. 5d). In the production epoch, the network adjusted the trajectory velocity to produce different intervals (Figs. S4a, b). This consistency of firing profile preservation in timed spatial reproduction and timed decision-making tasks implies that profile preservation is a universal computational scheme for neural networks to co-process time and other information.

A classic model of decision making requires two neuronal populations with mutual inhibition [33]. To understand the structure of the network that supported the co-functioning of time perception and decision making, we classified strongly active neurons at time point t_0 in the perception epoch into two types, c -increasing or c -decreasing, according to whether their firing rates at t_0 increased or decreased with c . We then chose a strongly active neuron as a reference, ordered its peak time with other strongly active neurons \mathcal{N} of the same or different types (see Methods), and then studied the connections $W(\Delta)$ from the reference neuron to \mathcal{N} , with Δ being the difference of the peak-time order from the reference. We found that if the reference and \mathcal{N} were of the same type, then $W(\Delta) > 0$ when Δ was slightly larger than θ and $W(\Delta) < 0$ otherwise (Fig. 5e, blue line): these asymmetric recurrent connections drove sequential firing of neurons of the same type. If the reference and \mathcal{N} were of different types, $W(\Delta) \approx 0$ only when $\Delta \approx 0$, and $W(\Delta) < 0$ otherwise (Fig. 5e, orange line), suggesting inhibition between them. This inhibition domination reflects the competition between the two firing sequences of two types of neurons [33]. To understand another functional implication of this inhibition profile, now consider a c -increasing neuron peaked at t_0 : it gave strong inhibition to c -decreasing neurons that peaked both before and after t_0 , except for c -decreasing neurons that peaked near t_0 . Therefore, only the c -decreasing neurons that peaked near t_0 were excitable, whereas c -decreasing neurons that peaked both too far ahead or lagged behind in time were not excitable due to this inhibition. This helped two neurons with an average timing preference at t_0 in the two firing sequences to be active more simultaneously under noises, which improved the precision and consistency of the temporal code in different simulation trials.

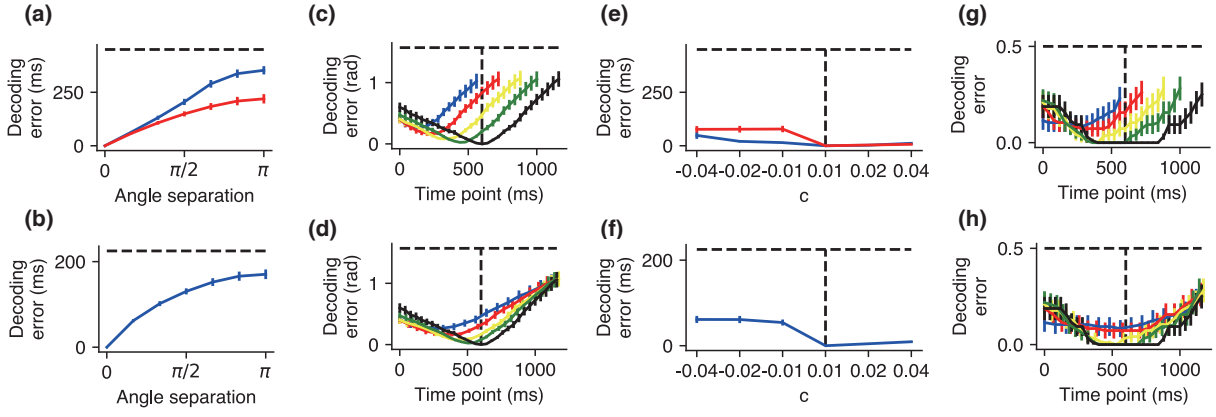


Figure 6: **Decoding generalizability.** (ad) Timed spatial reproduction task. (a) Decoding error of the time elapsed from the beginning of an epoch as a function of $|\theta_{train} - \theta_{test}|$. Training and testing using neuronal activities in the perception (blue) or production (red) epoch. Horizontal dashed line indicates chance level. (b) Decoding error of the duration of the perception epoch as a function of $|\theta_{train} - \theta_{test}|$. Training and testing using neuronal activities at the end of the delay epoch. (c) Decoding error of direction as a function of the time lapsed from the beginning of the production epoch. Training using neuronal activities at time 600 ms (t_1) after the beginning of the production epoch (vertical dashed line) when the to-be-produced interval is 1200 ms (T_1). Testing using neuronal activities at time points in the production epoch when the to-be-produced interval (T_2) is 600 ms (blue), 750 ms (red), 900 ms (yellow), 1050 ms (green), and 1200 ms (black). (d) The same as panel c, except that the maximal horizontal values of all the colored lines are scaled to $T_1 = 1200$ ms. With ideal temporal scaling, these lines should overlap after scaling. (eh) Timed decision-making task. (e) Decoding error of the time elapsed from the beginning of an epoch as a function of c in the perception (blue) or production (red) epoch. Training using neuronal activities at $c = 0.01$ (vertical dashed line), testing using other c values. (f) Decoding error of the duration of perception epoch as a function of c . Training using neuronal activities at the end of the delay epoch at $c = 0.01$ (vertical dashed line). Testing using neuronal activities at the end of the delay epoch at other c values. (g, h) Similar to panels c, d but for decoding error of decision choice. In panels a, c, e, f, $T = 1200$ ms. In all panels, error bars indicate s.e.m.

Decoding generalizability

A possible functional advantage of profile preservation is decoding generalizability. Because the coding of non-time information does not interfere with the coding of time, a decoder trained to read time information at specific non-time information should have above-chance performance at other non-time information. To validate this hypothesis, we trained a simple nearest-centroid decoder [34] using neuronal activities in our model. This decoder, after being trained by population state $\mathbf{f}(s)$ as a function of parameter s , read the value of s from a given state \mathbf{f}_0 to be the value that minimized the distance between $\mathbf{f}(s)$ and \mathbf{f}_0 . Using neuronal activities in a timed spatial reproduction task, we trained the decoder to read time (or time interval) at direction θ_{train} and tested its performance at direction θ_{test} . Although the performance decayed with $|\theta_{train} - \theta_{test}|$, it stayed above chance even when $|\theta_{train} - \theta_{test}| = \pi$ (Figs 6a, b).

Additionally, in the production epoch, neuronal activities temporally scaled with the time interval to be produced (Figs 2k, l, Fig. S3b, c). Consistently, if when the duration of the to-be-produced interval is T_1 , a decoder was trained to read direction at time t_1 from the beginning of the production epoch, then when the duration of the to-be-produced interval was changed to T_2 , it was best at reading direction at time t_2 , with $t_1/T_1 \approx t_2/T_2$ (Figs. 6c, d).

We also studied decoding in the timed decision-making task and found similar results (Figs 6eh). Together, the coding strategy of time implies two types of decoding generalizability: (1) the generalization of decoding time information across non-time information and (2) temporal scaling generalization across to-be-produced intervals.

Discussion

In summary, neural networks perceive time intervals through stereotypical dynamic trajectories, maintain time intervals by attractor dynamics in a complementary monotonic coding scheme, and adjust the evolution velocity of population activity to perform interval production or comparison. Spatial information or decision choice preserves neuronal firing profiles with temporal flow or time intervals. Decision making is combined with time perception through two firing sequences with mutual inhibition. Our results systematically summarize the computational principles of basic or combined time processing, which facilitate decoding generalizability.

Physically, time is consistently flowing, regardless of tasks. Therefore, it would be desirable for the brain to develop a consistent understanding of time across different non-time information (say, spatial information or decision choice). As we have shown, profile preservation facilitates the ability to read time information across different non-time information using a fixed set of decoding weights instead of using different sets of weights at different situations. Interestingly, the preservation of temporal profiles across non-time information was also observed in the prefrontal cortex even in tasks where time information was not required (Extended Data Fig. 3 of Ref. [21]). In the delay epoch of timed spatial reproduction or timed decision-making task in this paper, temporal flow did not need to be recorded neither, but the neuronal temporal profiles still tended to preserve

across non-time information (**Figs. S3d, S4c**). Thus, profile preservation should not need strong conditions to emerge during training. It has been proposed that the brain has a partially shared timing mechanism, which includes core timing regions (say, basal ganglia and supplementary motor area) that are consistently involved in temporal processing across contexts and areas that are activated in a context-dependent fashion [1]. If the brain indeed develops a consistent sense of time across contexts, then profile preservation, or generalizable representation of time across contexts, should be a computational principle, especially in core timing regions.

Another interesting question is how time information influences the coding of non-time information. To this end, we compared the coding of direction or decision choice at different time points (or time intervals) t_1 and t_2 . Although the similarity between non-time information decayed with $|t_1 - t_2|$, it stayed above chance most of time (**Fig. S5a, b, e, f**); so did the performance of a decoder trained at time t_1 and tested at t_2 (**Fig. S5c, d, g, h**). Therefore, at least in our model, the coding of time and non-time information was, to some extent, orthogonal: they did not strongly interfere with each other. The decoding generalizability of non-time information across time has been studied in working memory tasks [34, 35] and has been considered an advantage of working memory models in which information is maintained in stable, or a stable subspace of, neuronal activity [34, 36]. However, in these tasks, time information was not required to be recorded. The decoding generalizability of time information across non-time information is, to our knowledge, also in lack of research. Therefore, experimental studies on the co-processing of time and non-time information are strongly recommended, especially in the prefrontal and parietal cortices which are deeply involved in spatial working memory and decision making [17, 18].

The scaling of state evolution velocity to produce intervals has been observed in animal experiments [37, 14, 25]. As suggested by temporal scaling of decoding performance (**Figs. 6c, d, g, h**), such tuning of evolution velocity provides a temporally compressed or dilated interpretation of the physical flow of time. For example, at two different evolution velocities v_1 and v_2 , the network may reach similar states at times t_1 and t_2 (with $v_1 t_1 = v_2 t_2$) after a cue, so that the network may generate similar movements or respond similarly to an external stimulus. In other words, t_1 and t_2 have similar meaning to the network, even if they are physically not equal. Due to this temporal scaling, people can adjust their internal clock speed to recognize or produce temporally compressed or dilated speech, music, or sequence of finger movements [38, 39, 40].

A number of biologically plausible neural mechanisms to code temporal flow have been proposed, including accumulating firing [9, 10], synfire chains [11, 12], and the beating of a range of oscillation frequencies [13]. Our results suggest that there are computational principles that should be added to these mechanisms for more complete timing models, which may include neural mechanisms to improve noise robustness of state trajectories for precise time perception, control trajectory velocity for temporal pattern recognition or production, and process spatial information or decision making in a subspace of network state orthogonal with the subspace that processes time. Understanding these mechanisms of time processing in working memory is of great interest for future research.

Methods

The methods of analysis and models are provided in the SI Text.

Acknowledgment

This work was supported by Hong Kong Baptist University (HKBU) Strategic Development Fund and HKBU Research Committee and Interdisciplinary Research Clusters Matching Scheme 2018/19 (RC-IRCMs/18-19/SCI01). This research was conducted using the resources of the High-Performance Computing Cluster Centre at HKBU, which receives funding from the RGC and HKBU.

References

- [1] H. Merchant, D. L. Harrington, and W. H. Meck, "Neural basis of the perception and estimation of time," *Annu. Rev. Neurosci.*, vol. 36, pp. 313–336, 2013.
- [2] M. J. Allman, S. Teki, T. D. Griffiths, and W. H. Meck, "Properties of the internal clock: First- and second-order principles of subjective time," *Annu. Rev. Psychol.*, vol. 65, pp. 1–29, 2014.
- [3] J. J. Paton and D. V. Buonomano, "The neural basis of timing: Distributed mechanisms for diverse functions," *Neuron*, vol. 98, pp. 687–705, 2018.
- [4] E. A. Petter, S. J. Gershman, and W. H. Meck, "Integrating models of interval timing and reinforcement learning," *Trends Cogn. Sci.*, vol. 22, pp. 911–922, 2018.
- [5] C. Constantinidis and T. Klingberg, "The neuroscience of working memory capacity and training," *Nat. Rev. Neurosci.*, vol. 17, pp. 438–449, 2016.
- [6] A. Baddeley, "Working memory: Theories, models, and controversies," *Annu. Rev. Psychol.*, vol. 63, pp. 1–29, 2012.
- [7] M. D. Mauk and D. V. Buonomano, "The neural basis of temporal processing," *Annu. Rev. Neurosci.*, vol. 27, p. 307, 2004.
- [8] C. V. Buhusi and W. H. Meck, "What makes us tick? Functional and neural mechanisms of interval timing," *Nat. Rev. Neurosci.*, vol. 6, pp. 755–765, 2005.
- [9] M. Treisman, "Temporal discrimination and the indifference interval. Implications for a model of the "internal clock"," *Psychol. Monogr.*, vol. 77, pp. 1–31, 1963.
- [10] P. R. Killeen and J. G. Fetterman, "A behavioral theory of timing," *Psychol. Rev.*, vol. 95, pp. 274–295, 1988.

- [11] R. H. R. Hahnloser, A. A. Kozhevnikov, and M. S. Fee, “An ultra-sparse code underlies the generation of neural sequence in a songbird,” *Nature*, vol. 419, p. 6570, 2002.
- [12] G. F. Lynch, T. S. Okubo, A. Hanuschkin, R. H. R. Hahnloser, and M. S. Fee, “Rhythmic continuous-time coding in the songbird analog of vocal motor cortex,” *Neuron*, vol. 90, pp. 877–892, 2016.
- [13] M. S. Matell and W. H. Meck, “Cortico-striatal circuits and interval timing: coincidence detection of oscillatory processes,” *Brain Res. Cogn. Brain Res.*, vol. 21, pp. 139–170, 2004.
- [14] J. W. D. Narain, E. A. Hosseini, and M. Jazayeri, “Flexible timing by temporal scaling of cortical responses,” *Nat. Neurosci.*, vol. 21, pp. 102–110, 2018.
- [15] S. Teki and T. D. Griffiths, “Working memory for time intervals in auditory rhythmic sequences,” *Front. Psychol.*, vol. 5, p. 1329, 2014.
- [16] R. B. Ivry and J. E. Schlerf, “Dedicated and intrinsic models of time perception,” *Trends Cogn. Sci.*, vol. 12, pp. 273–280, 2008.
- [17] A. H. Lara and J. D. Wallis, “The role of prefrontal cortex in working memory: A mini review,” *Front. Syst. Neurosci.*, vol. 9, p. 173, 2015.
- [18] J. I. Gold and M. N. Shadlen, “The neural basis of decision making,” *Annu. Rev. Neurosci.*, vol. 30, pp. 535–574, 2007.
- [19] H. Hong, D. L. K. Yamins, N. J. Majaj, and J. J. DiCarlo, “Explicit information for category-orthogonal object properties increases along the ventral stream,” *Nat. Neurosci.*, vol. 19, pp. 613–622, 2016.
- [20] H. F. Song, G. R. Yang, and X.-J. Wang, “Training excitatory-inhibitory recurrent neural networks for cognitive tasks: A simple and flexible framework,” *PLoS Comp. Bio.*, vol. 12, p. e1004792, 2016.
- [21] V. Mante, D. Sussillo, K. V. Shenoy, and W. T. Newsome, “Context-dependent computation by recurrent dynamics in prefrontal cortex,” *Nature*, vol. 503, pp. 78–84, 2013.
- [22] D. Sussillo, M. M. Churchland, M. T. Kaufman, and K. V. Shenoy, “A neural network that finds a naturalistic solution for the production of muscle activity,” *Nat. Neurosci.*, vol. 18, pp. 1025–1033, 2015.
- [23] G. R. Yang, M. R. Joglekar, H. F. Song, W. T. Newsome, and X.-J. Wang, “Task representations in neural networks trained to perform many cognitive tasks,” *Nat. Neurosci.*, vol. 22, pp. 297–306, 2019.
- [24] A. E. Orhan and W. J. Ma, “A diverse range of factors affect the nature of neural representations underlying short-term memory,” *Nat. Neurosci.*, vol. 22, pp. 275–283, 2019.
- [25] E. D. Remington, D. Narain, E. A. Hosseini, and M. Jazayeri, “Flexible sensorimotor computations through rapid reconfiguration of cortical dynamics,” *Neuron*, vol. 98, pp. 1005–1019, 2018.
- [26] L. F. Abbott and F. S. Chance, “Drivers and modulators from push-pull and balanced synaptic input,” *Prog. Brain Res.*, vol. 149, pp. 147–155, 2005.
- [27] U. R. Karmarkar and D. V. Buonomano, “Timing in the absence of clocks: Encoding time in neural network states,” *Neuron*, vol. 53, pp. 427–438, 2007.
- [28] H. S. Seung, “How the brain keeps the eyes still,” *Proc. Natl. Acad. Sci. USA*, vol. 93, pp. 13339–13344, 1996.
- [29] R. Romo, C. D. Brody, A. Hernandez, and L. Lemus, “Neuronal correlates of parametric working memory in the prefrontal cortex,” *Nature*, vol. 399, pp. 470–473, 1999.
- [30] A. Goel and D. V. Buonomano, “Temporal interval learning in cortical cultures is encoded in intrinsic network dynamics,” *Neuron*, vol. 91, pp. 1–8, 2016.
- [31] C. J. MacDonald, K. Q. Lepage, U. T. Eden, and H. Eichenbaum, “Hippocampal ‘time cells’ bridge the gap in memory for discontinuous events,” *Neuron*, vol. 71, pp. 737–749, 2011.
- [32] D. Ji and M. A. Wilson, “Coordinated memory replay in the visual cortex and hippocampus during sleep,” *Nat. Neurosci.*, vol. 10, pp. 100–107, 2007.
- [33] X.-J. Wang, “Probabilistic decision making by slow reverberation in cortical circuits,” *Neuron*, vol. 36, pp. 955–968, 2002.
- [34] J. D. M. et al, “Stable population coding for working memory coexists with heterogeneous neural dynamics in prefrontal cortex,” *Proc. Natl. Acad. Sci. USA*, vol. 114, pp. 394–399, 2017.
- [35] M. G. Stokes, M. Kusunoki, N. Sigala, H. Nili, D. Gaffan, and J. Duncan, “Dynamic coding for cognitive control in prefrontal cortex,” *Neuron*, vol. 78, pp. 364–375, 2013.
- [36] S. Druckmann and D. B. Chklovskii, “Neuronal circuits underlying persistent representations despite time varying activity,” *Curr. Biol.*, vol. 22, pp. 2095–2103, 2012.
- [37] S. Shinomoto, T. Omi, A. Mita, H. Mushiake, K. Shima, Y. Matsuzaka, and J. Tanji, “Deciphering elapsed time and predicting action timing from neuronal population signals,” *Front. Comput. Neurosci.*, vol. 5, p. 29, 2011.
- [38] R. Gütig and H. Sompolinsky, “Time-warpinvariant neuronal processing,” *PLoS Biol.*, vol. 7, p. e1000141, 2009.
- [39] V. Goudar and D. V. Buonomano, “Encoding sensory and motor patterns as time-invariant trajectories in recurrent neural networks,” *eLife*, vol. 7, p. e31134, 2018.
- [40] N. F. Hardy, V. Goudar, J. L. Romero-Sosa, and D. V. Buonomano, “A model of temporal scaling correctly predicts that motor timing improves with speed,” *Nat. Commun.*, vol. 9, p. 4732, 2018.